

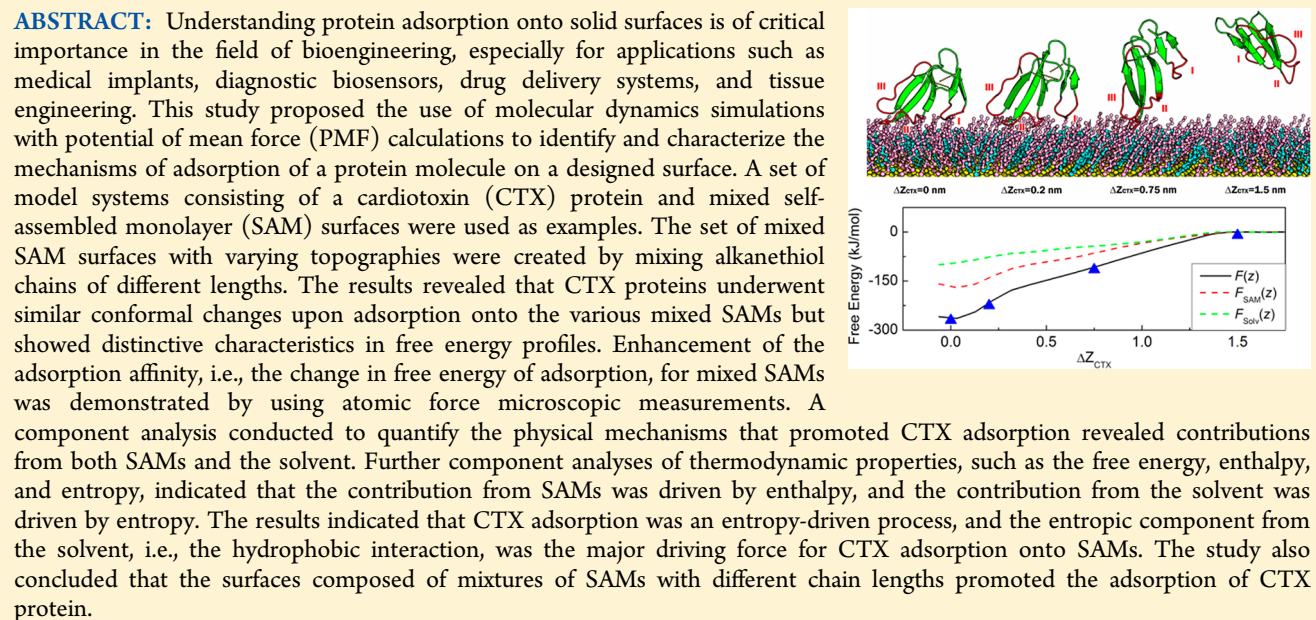
Thermodynamic Investigations Using Molecular Dynamics Simulations with Potential of Mean Force Calculations for Cardiotoxin Protein Adsorption on Mixed Self-Assembled Monolayers

Shih-Wei Hung,[†] Pai-Yi Hsiao,[†] Ming-Chang Lu,[‡] and Ching-Chang Chieng*,^{†,§}

[†]Department of Engineering and System Science, National Tsing Hua University, Hsinchu, Taiwan

[‡]Department of Mechanical Engineering, National Chiao Tung University, Hsinchu, Taiwan

[§]Department of Mechanical and Biomedical Engineering, City University of Hong Kong, Kowloon, Hong Kong



INTRODUCTION

When a solid surface comes into contact with a biological environment, the surface is spontaneously coated with proteins. The resulting adsorbed protein layer, which is influenced by the surface properties, plays a key role in determining cellular responses. Thus, the understanding of protein adsorption onto solid surfaces is of critical importance in the field of bioengineering, including applications such as medical implants, diagnostic biosensors, drug delivery systems, and tissue engineering.^{1–4} To identify the critical elements in the protein–surface system, a well-defined model surface is required to reduce the compositional complexity of the biological surface.

Self-assembled monolayers (SAMs) have been developed as excellent model surfaces because they are stable, highly ordered, easy to prepare, and provide a wide range of organic functionality.⁵ The influence of surface chemical functionalities on protein adsorption, cellular behavior, and tissue responses has been extensively investigated and reviewed by Thevenot et al.² Recent advances in surface chemistry revealed that the

hydrophobic methyl group ($-\text{CH}_3$) promotes protein adsorption. It is generally accepted that hydrophobic interactions are the major mechanism for protein adsorption onto surfaces.^{4,6–10} Because water is a polar molecule, contact between water and hydrophobic (nonpolar) surfaces increases the extent of self-association within the neighboring water molecules and creates an entropic penalty. Thus, the dehydration of both proteins and hydrophobic surfaces provide an entropic driving force for protein adsorption.^{4,9} In addition to their functionalities, the topographies of surfaces also influence protein adsorption. Increased surface roughness and topological features provide increased surface area for protein adsorption.¹¹

Although the behavior of protein adsorption has been intensively studied, detailed mechanisms at the molecular level remain limited due to experimental constraints. Molecular

Received: May 15, 2012

Revised: September 25, 2012

Published: September 26, 2012

dynamics (MD) simulations have been used as a direct approach to address protein–surface interactions and protein conformational transitions for protein adsorption onto solid surfaces and have been reviewed in a number of publications.^{12–14} In recent years, MD simulations have also been extensively implemented to investigate the atomic-resolution details,^{15–23} such as orientation, structure, dynamics, interfacial water behavior, and driving force, of protein adsorption onto SAMs. However, experiments have revealed that in addition to the protein–surface interaction, entropic effects, such as hydrophobic interactions, are also critical factors in the protein adsorption process.^{4,6,8} Therefore, a thermodynamic analysis is needed to thoroughly understand the protein adsorption process. As shown by MD simulations, one important thermodynamic quantity characterizing the dynamic process is the potential of mean force (PMF),²⁴ which is the equilibrium free energy difference along the reaction coordinate. Free energy calculations can provide information on the microscopic and thermodynamic aspects of biologically dynamic processes. For example, free energy calculations have been applied to a wide range of chemical and biological systems, including the study of protein–ligand associations, solvation free energy, transport phenomena, as well as protein folding and stability, and have been reviewed in detail.^{25,26} Thus, PMF calculations are a valuable approach to identifying and quantifying the thermodynamics and major mechanisms of protein adsorption onto a surface.

Cardiotoxins (CTXs), small basic proteins that are abundantly present in snake venom, exhibit physiological activities including hemolysis, cytotoxicity, and the depolarization of muscles.^{27,28} Due to their highly diverse pharmacological effects, the interactions between CTXs and membranes have been investigated extensively by using various methods including Fourier transform infrared spectroscopy,^{29,30} nuclear magnetic resonance (NMR) spectroscopy,^{31,32} and computer simulations.^{33–35} These studies revealed that the hydrophobic tips of the characteristic three-fingered loops of CTXs play an important role in their interaction with membranes. The three-dimensional structure of CTX homologues in both aqueous and micellar environments is available,^{31,36} and the interactions between CTXs and lipid membranes have been well studied. Thus, CTX was chosen as the model protein to investigate the interaction of protein adsorption onto hydrophobic surfaces.

In the present study, MD simulations were performed to study the adsorption free energy of a single CTX onto CH_3 -terminated SAM surfaces with various topographies, which were created by mixing *n*-alkanethiol of different chain lengths. The simulated adsorption process provided molecular insights into the protein adsorption mechanism. The decomposition of free energy into enthalpic and entropic contributions was implemented to understand the thermodynamic driving forces of protein adsorption. Furthermore, free energy component analyses were performed to determine the effects of both the SAMs and the solvent on the adsorption process.

SIMULATION METHODOLOGIES

Model System and Computational Details. The model system in the present study consisted of a single CTX A3 protein molecule on SAMs in the presence of explicitly defined water molecules and ions (Figure 1). This work sought to study the protein adsorption mechanisms on mixed SAMs having a consistent tail group but different chain lengths. A recent study³⁷ revealed that the water adsorption properties do not

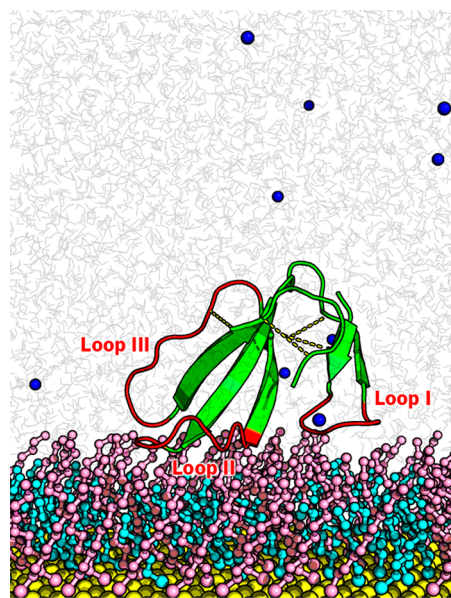


Figure 1. The molecular model system consisting of a single CTX protein, a mixed SAM surface of $\text{S}(\text{CH}_2)_5\text{CH}_3$ (C5, in cyan) and $\text{S}(\text{CH}_2)_9\text{CH}_3$ (C9, in pink) molecules, and the solvent medium with explicit water molecules and counterions (blue spheres). The three characteristic loops of CTX are shown in red. The yellow dashed lines indicate the disulfide bonds. The sizes of the different molecules are not to scale. The molecular images in this paper were created by using Pymol.⁶¹

differ on $(\text{CH}_2)_7\text{CH}_3$ and mixed $(\text{CH}_2)_5\text{CH}_3/(\text{CH}_2)_7\text{CH}_3$ SAMs, which is in contrast to the results of Rudich et al.³⁸ that the amount of adsorbed water increases with surface roughness with mixed $(\text{CH}_2)_{12}\text{CH}_3/(\text{CH}_2)_{18}\text{CH}_3$ and mixed $(\text{CH}_2)_{18}\text{CH}_3/(\text{CH}_2)_{22}\text{CH}_3$ SAMs. These findings suggested that the adsorption behavior is affected by the degree of roughness resulting from the difference in the chain lengths of mixed SAMs. In order to investigate the enhancement of protein adsorption onto mixed SAMs, two types of alkanethiol chains with sufficient chain length difference, $\text{S}(\text{CH}_2)_5\text{CH}_3$ (C5) and $\text{S}(\text{CH}_2)_9\text{CH}_3$ (C9), were chosen to comprise the mixed SAMs. The SAMs were modeled by generating a 12×12 array of the single chain with a $\sqrt{3} \times \sqrt{3}\text{R}30^\circ$ lattice structure and a sulfur–sulfur spacing of 0.497 nm. Each lattice point was occupied by an alkanethiol chain of either C5 or C9. Five mixing ratios, $\chi_{\text{C9}} = 0, 0.25, 0.5, 0.75$, and 1, were studied, where χ_{C9} was defined as $N_{\text{C9}}/(N_{\text{C5}} + N_{\text{C9}})$ with N_{C5} and N_{C9} representing the number of C5 and C9 chains, respectively. The Au(111) substrate was modeled as a single layer of gold atoms. The scanning tunneling microscopy topology showed that *n*-decanethiol ($\text{CH}_3(\text{CH}_2)_{10}\text{SH}$) and *n*-dodecanethiol ($\text{CH}_3(\text{CH}_2)_{11}\text{SH}$) were randomly distributed in the mixed SAM,³⁹ thereby indicating that mixed SAMs with molecules of similar composition would not undergo phase separation.⁴⁰ Moreover, it was shown that the molecular-scale uniformity of mixed SAMs with different chain lengths can be prepared experimentally.⁴¹ Therefore, a homogeneous mixture of the mixed SAMs was assumed, and the mixed SAMs were generated by randomly placing C5 and C9 molecules on the gold substrate. The NMR three-dimensional structure of CTX A3, comprised of 60 amino acid residues, was obtained from the Protein Data Bank (1I02).³⁶ The CTX-SAM system was solvated in a rectangular box ($5.99 \times 5.19 \times 7.00$ nm) in a bath of water molecules with a density of 1000 kg/m^3 . To maintain

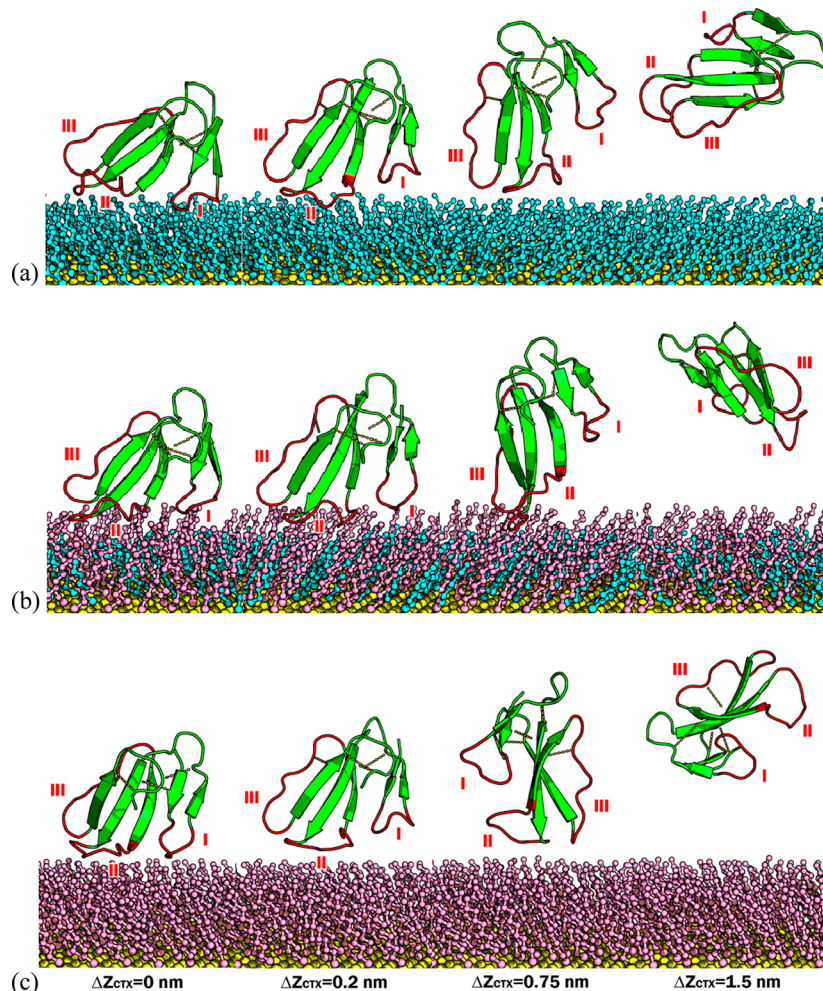


Figure 2. Snapshots of CTX conformations at $\Delta z_{\text{CTX}} = 0$ (adsorbed state, the 1st stage), 0.2 (the 1st stage), 0.75 (the 2nd stage), and 1.5 nm (the 3rd stage) on (a) pure C5 SAMs with $\chi_{\text{C9}} = 0$, (b) mixed SAMs with $\chi_{\text{C9}} = 0.5$, and (c) pure C9 SAMs with $\chi_{\text{C9}} = 1.0$. Water molecules are not shown to provide a clear illustration.

the electroneutrality of the system, one Na^+ ion and ten Cl^- ions were added to the simulation box. The periodic boundary conditions and minimum image convention were applied in the x and y directions. A virtual wall was placed on top of the simulation box to confine the system. Previous experimental studies^{29,30} and computer simulations^{42,43} confirmed that the most favorable orientation of CTX A3 proteins binding to membranes was with the three-finger loops facing the surface. Therefore, to conserve computing time, the CTX protein configuration was initially set with the three-finger loops facing the SAM surface.

The interactions within the CTX protein were described by the GROMOS-96(43a2) force field.⁴⁴ For the alkanethiol chains in the SAMs, the Huatman and Klein united atom model⁴⁵ was used. The interaction between the SAM chains and the gold surface was described by the Lennard-Jones (LJ) 12–3 potential.⁴⁶ Water molecules were modeled by using the extended simple point charge model.⁴⁷ The cross parameters of the LJ interactions were calculated by the combination rule of the geometric mean.

All of the simulations were performed with the GROMACS program.⁴⁴ The simulations were performed in a canonical ensemble with integrating time steps of 1.0 fs, and the temperature was controlled by a Nose–Hoover thermostat^{48,49} with a time constant of 0.02 ps. All of the covalent bonds were

constrained by the LINCS algorithm.⁵⁰ For the nonbonded van der Waals (vdW) interactions, a cutoff distance of 1.5 nm was used. The electrostatic interaction was limited to 2.5 nm by a force-shifted function. Previous studies^{51,52} demonstrated that the force-shifted spherical cutoff method for the electrostatic interaction correctly modeled the dynamics of biomolecules in solutions.

PMF Calculation. The PMF is an important thermodynamic function used to characterize the CTX adsorption process.⁵³ Moreover, the thermodynamics components, such as the free energy, enthalpy, and entropy, can be extracted from the PMF profile to quantify contributions to the adsorption process. Thus, the umbrella sampling method⁵⁴ was implemented to calculate the PMFs of CTX on various mixed SAMs for the present study. A set of separate umbrella simulations were performed, using a harmonic potential $u_i(z_i)$ applied through the center of mass of CTX at the i th window (window size of 0.05 nm) along the z coordinate. The harmonic potentials were presented by

$$u_i(z_i) = \frac{1}{2}k(z_{\text{CTX}} - z_i) \quad (1)$$

where k is the force constant, z_{CTX} is the z coordinate of the CTX protein, and z_i is the center position of the i th window. According to the well-known Boltzmann distribution of a

harmonically bound particle, the position fluctuations are related to the force constant, k , through $k_B T/k$, where k_B is the Boltzmann constant and T is the absolute temperature. Thus, the force constant, k , was chosen to be $376 k_B T/\text{nm}^2$ such that the position fluctuations are similar to the window size (0.05 nm), thereby resulting in sufficient overlap over the umbrella sampling windows. The 40 independent configurations for 40 windows with different initial separation distances were created to cover the entire distance of interest. For each window, an equilibrium run was conducted for 4 ns followed by an additional 4 ns production run. All of the mean forces acting on the CTX, $\langle f(z') \rangle$, were collected in the production runs for PMF calculations.

The free energy profile, $F(z)$, which corresponds to the PMF, is the reversible thermodynamic work along a coordinate z relative to some reference value z_0 . Because PMF is the reversible work enacted along the reaction coordinate, PMF can present both adsorption and desorption processes. For the sake of simplicity, only the adsorption process will be illustrated and described in the remainder of this paper. The PMF was calculated by integrating $\langle f(z') \rangle$ along the z direction:

$$F(z) = F(z_0) - \int_{z_0}^z \langle f(z') \rangle dz' \quad (2)$$

where $F(z_0)$ is arbitrarily chosen as a reference state at the reference position z_0 . The PMF represents only relative values; therefore, in the present study, $F(z_0)$ was chosen to be zero in the state where there was no interaction between the CTX and SAM. To compare the PMFs for different SAMs, the coordinate of the center of mass of the CTX, Δz_{CTX} , was shifted such that the free energy was at a minimum at $\Delta z_{\text{CTX}} = 0$. The value of Δz_{CTX} can also express the separation distance between the CTX and SAMs.

The mean force can be linearly decomposed into a sum of components and allows us to distinguish contributions originating from different interactions. In the present study, the free energy contributions from the solvent (water molecules and ions) and SAM components were of interest. Therefore, the total PMF was decomposed into solvent and SAM contributions, and the component analysis was conducted according to

$$\begin{aligned} F(z) &= F_{\text{Solv}}(z) + F_{\text{SAM}}(z) \\ &= \left(- \int_{z_0}^z \langle f_{\text{Solv}}(z') \rangle dz' \right) + \left(- \int_{z_0}^z \langle f_{\text{SAM}}(z') \rangle dz' \right) \end{aligned} \quad (3)$$

where f_{Solv} and f_{SAM} are the mean forces acting on the CTX from the solvent and from the SAM, respectively.

RESULTS AND DISCUSSION

Orientations and Conformational Changes of CTX Adsorption. The snapshots of CTX in the adsorbed state ($\Delta z_{\text{CTX}} = 0$) are shown in Figure 2. The orientations of CTX in the adsorbed state are consistent with our previous study⁵⁵ that the CTX is adsorbed onto SAMs by the three hydrophobic loops for various SAMs. Besides $\Delta z_{\text{CTX}} = 0$, three snapshots of CTX conformations at three separation distances ($\Delta z_{\text{CTX}} = 0.2$, 0.75, and 1.5 nm) represent the three stages of CTX adsorption onto pure C5 SAMs (Figure 2a): the first stage where all three loops are attached to the C5 surface ($\Delta z_{\text{CTX}} = 0$ and 0.2 nm); the second stage where only Loop I departed from the SAM surface ($\Delta z_{\text{CTX}} = 0.75$ nm); and the third stage in which all

three loops were a distance from the SAM surface with no specific orientation of the CTX molecule in the bulk solvent environment ($\Delta z_{\text{CTX}} = 1.5$ nm). The snapshots of CTX adsorption processes are shown in parts b and c of Figure 2 for the well-mixed SAMs with half C9 and half C5 ($\chi_{\text{C9}} = 0.5$) and for the pure C9 SAMs.

The radius of gyration (R_{gyr}) was calculated to further understand the conformational change of CTX protein during the adsorption process. The R_{gyr} profiles (Figure 3) are

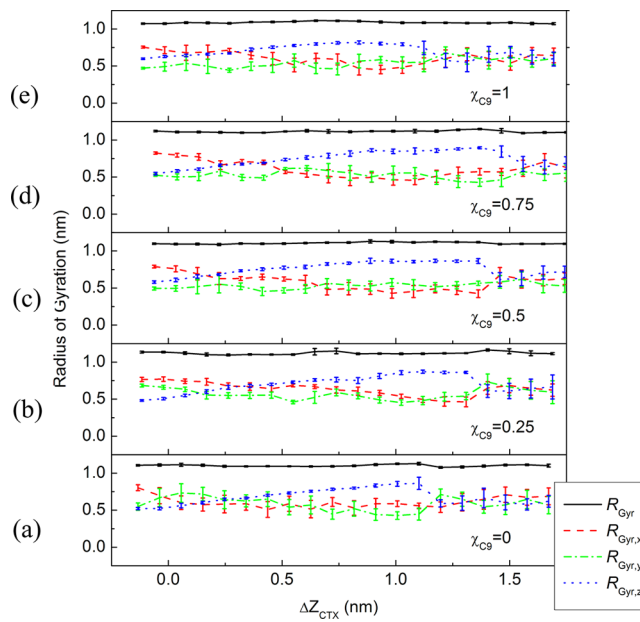


Figure 3. Radius of gyration profiles (black solid line) and the components in x (red dashed line), y (green dashed-dotted line), and z (blue dotted line) directions of CTX protein onto SAMs with mixing ratios of (a) $\chi_{\text{C9}} = 0$, (b) $\chi_{\text{C9}} = 0.25$, (c) $\chi_{\text{C9}} = 0.5$, (d) $\chi_{\text{C9}} = 0.75$, and (e) $\chi_{\text{C9}} = 1$.

consistent for various SAMs, which indicate the CTX proteins undergo similar conformational changes during adsorption onto various SAMs. The $R_{\text{gyr},x}$, $R_{\text{gyr},y}$, and $R_{\text{gyr},z}$ profiles depict the deformation of CTX protein in x , y , and z directions. In the first and second stages, the increasing values of $R_{\text{gyr},z}$ (blue dotted lines) with increasing separation distance suggest that the CTX is elongated in the z direction, which is in agreement with the snapshots (Figure 2). The smaller fluctuations in $R_{\text{gyr},z}$ than in $R_{\text{gyr},x}$ and $R_{\text{gyr},y}$ imply the CTX is more confined in the z direction. In the third stage, the values of $R_{\text{gyr},x}$, $R_{\text{gyr},y}$, and $R_{\text{gyr},z}$ are similar because there is no specific orientation of the CTX molecule. In addition to conformational analysis, PMF analysis was further implemented to determine the performance of CTX adsorption on different SAM surfaces.

Potential of Mean Force. The analyzed PMFs provide the thermodynamic functions of the states, such as the free energy, enthalpy, and entropy, of the process. These thermodynamic properties will be calculated and discussed in this paper. The black solid lines in Figure 4 display the total free energy profiles ($F(\Delta z_{\text{CTX}})$) as the CTX protein leaves the various SAMs surfaces at different separation distances (Δz_{CTX}). The components of the total free energy attributed to the SAMs (F_{SAM}) as well as the solvent (F_{Solv}) are depicted in Figure 4 as red dashed lines and green dashed-dotted lines, respectively. The negative values of $F(\Delta z_{\text{CTX}})$, $F_{\text{SAM}}(\Delta z_{\text{CTX}})$, and $F_{\text{Solv}}(\Delta z_{\text{CTX}})$ with decreasing separation distance indicate that

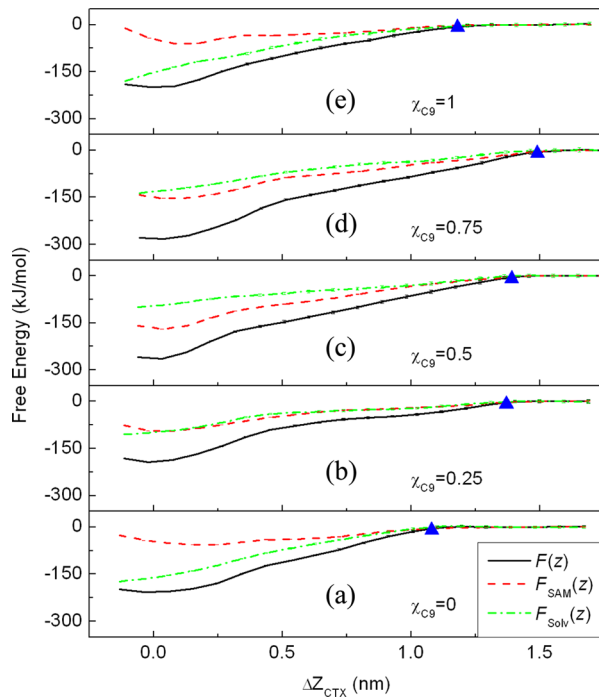


Figure 4. Total free energy profiles (black solid line) and the corresponding contributions from the SAMs (red dashed line) and the solvent (green dashed-dotted line) for SAM mixing ratios of (a) $\chi_{\text{C9}} = 0$, (b) $\chi_{\text{C9}} = 0.25$, (c) $\chi_{\text{C9}} = 0.5$, (d) $\chi_{\text{C9}} = 0.75$, and (e) $\chi_{\text{C9}} = 1$. Blue triangles indicate the positions at which the CTX molecule detaches from the SAMs.

CTX adsorption is a spontaneous process when the CTX protein is sufficiently close to the SAMs and that both the SAM and solvent components promote CTX adsorption. The $F(\Delta z_{\text{CTX}})$ profiles are similar in shape because the dynamic behaviors of CTX adsorption onto different SAMs are similar, as shown in Figure 2. The position at which $F(\Delta z_{\text{CTX}})/F(\Delta z_{\text{CTX}}=0) = 0.01$ is referred to as the detachment distance, which is labeled by using blue triangles in Figure 4. The detachment distances for SAMs with mixing ratios of $\chi_{\text{C9}} = 0, 0.25, 0.5, 0.75$, and 1 are $1.08, 1.37, 1.39, 1.49$, and 1.18 nm, respectively. Our previous study⁵⁵ demonstrated that the molecules of the outer layer formed in mixed SAMs are more flexible than those of pure SAMs. The flexible outer layer in mixed SAMs increased the distance interacting with the CTX protein, and the detachment distances for mixed SAMs are longer than those of pure SAMs, as shown in Figure 4. Thus, the free energy minima are different for the various mixed SAMs, which will be discussed in the following section.

The free energy change of the adsorption process (ΔF) is computed to quantify the adsorption affinity of the CTX onto SAM surfaces with different mixing ratios, where Δ indicates the change in the thermodynamic functions of state resulting from the adsorption process. ΔF was computed as

$$\Delta F = F_{\text{adsorbed-state}}(\Delta z_{\text{CTX}}) - F_{\text{bulk-state}}(\Delta z_{\text{CTX}}) \quad (4)$$

where $F_{\text{adsorbed-state}}(\Delta z_{\text{CTX}})$ is the free energy in the adsorbed state and has a value of $F(\Delta z_{\text{CTX}}=0)$. $F_{\text{bulk-state}}(\Delta z_{\text{CTX}})$ is the free energy of the CTX molecule in the bulk solvent state and is set to zero, i.e., $\Delta F_{\text{bulk-state}} \equiv F(\Delta z_{\text{CTX}}) = 0$. Equation 4 implies that ΔF is equivalent to the PMF minimum shown in Figure 4 and represents the adsorption affinity of the CTX protein onto the SAMs. The adsorption affinities indicated by ΔF for mixed

SAMs with mixing ratios of $\chi_{\text{C9}} = 0.5$ and 0.75 are approximately 35% higher than those on other SAMs surfaces (Figure 5). Atomic force microscopy measurements also

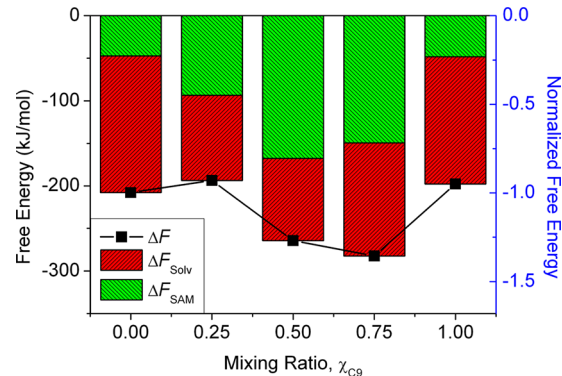


Figure 5. The change in free energy of the adsorption process and the corresponding contributions from the SAMs (green) and the solvent (red) as a function of the mixing ratio of C5 and C9. The normalized free energy (shown by the vertical axis on right) is defined as the ratio of the free energy on the SAMs to the free energy on the pure C5 SAMs ($\chi_{\text{C9}} = 0$).

indicated that the adhesion forces of CTX on mixed SAMs are larger than those on pure SAMs.⁵⁶ The contributions from the SAMs (ΔF_{SAM} shown in green) and the solvent (ΔF_{Solv} shown in red) are also displayed to distinctly indicate the driving forces for CTX adsorption onto SAMs surfaces. The green bars indicate that the contribution of SAMs to the adsorption affinity is significantly higher for mixed SAMs (i.e., 2.0-, 3.5-, and 3.2-fold higher at mixing ratios of 0.25, 0.5, and 0.75, respectively, relative to pure C5 SAMs). However, the red bars indicate that the contribution of the solvent to adsorption affinity is lower for mixed SAMs (i.e., 0.62-, 0.60-, and 0.83-fold lower at mixing ratios of 0.25, 0.5, and 0.75, respectively, relative to pure C5 SAMs). Thus, the overall driving force for CTX adsorption onto pure SAM surfaces is mainly contributed by the solvent ($\Delta F_{\text{Solv}}/\Delta F = 0.77$ and 0.76 for $\chi_{\text{C9}} = 0$ and 1 , respectively), whereas the driving force for CTX adsorption onto mixed SAM surfaces is mainly contributed by the SAMs ($\Delta F_{\text{Solv}}/\Delta F = 0.37$ for $\chi_{\text{C9}} = 0.5$) or the SAMs and the solvent equally ($\Delta F_{\text{Solv}}/\Delta F = 0.52$ and 0.47 for $\chi_{\text{C9}} = 0.25$ and 0.75 , respectively). The component opposite ΔF_{SAM} and ΔF_{Solv} trends degrades the enhancement of adsorption affinity using mixed SAMs. Further analyses were implemented to understand the adsorption mechanism of CTX onto SAMs with different mixing ratios.

Thermodynamics of CTX Adsorption. A decomposition of the free energies into enthalpic and entropic components, according to the thermodynamic relationship, $\Delta F = \Delta U - T\Delta S$, provides additional insights into the protein adsorption mechanisms. Because the change in internal energy, ΔU , can be approximated by the change in enthalpy, ΔH , in constant-NVT simulations and enthalpy is typically used in experiments. For the convenience of comparison with experiments, enthalpy was used instead of internal energy in this paper. The change in enthalpy of the adsorption process was calculated based on the change in the potential energy and the change in entropy is then obtained by the thermodynamic relationship. Our previous steered MD simulation⁵³ revealed that vdW interactions were the dominant type of interaction attributed to CTX adsorption onto SAMs when the electrostatic

interaction was held constant. Therefore, only vdW interactions from the SAMs and the solvent are considered in the enthalpy calculation for the present study. It has been shown that there is a linear relationship between the solute–solvent vdW interactions and the surface area of various peptides and proteins.⁵⁷ We have also found⁵⁵ that the vdW interaction energy between CTX and SAM molecules is related to the contact area between CTX and SAM in a linear manner when CTX is adsorbed onto SAMs without an external force. Thus, the profiles of both the changes in the enthalpies ($\Delta H_{\text{SAM}}(\Delta z_{\text{CTX}})$ and $\Delta H_{\text{Solv}}(\Delta z_{\text{CTX}})$) and the contact surface areas ($\Delta A_{\text{SAM}}(\Delta z_{\text{CTX}})$ and $\Delta A_{\text{Solv}}(\Delta z_{\text{CTX}})$) from different components during the adsorption process are further examined in the present study. The change in contact area is computed by using the double cubic lattice method⁵⁸ with a probe radius equal to 0.14 nm. The relationships between $\Delta H_{\text{SAM}}(\Delta z_{\text{CTX}})$ and $\Delta A_{\text{SAM}}(\Delta z_{\text{CTX}})$ and between $\Delta H_{\text{Solv}}(\Delta z_{\text{CTX}})$ and $\Delta A_{\text{Solv}}(\Delta z_{\text{CTX}})$ are shown in parts a and b of Figure 6, respectively. Both $\Delta H_{\text{SAM}}(\Delta z_{\text{CTX}})$ and

favor protein adsorption in enthalpy. The values of $\Delta H_{\text{Solv}}(\Delta z_{\text{CTX}})$ increase with decreasing $\Delta A_{\text{Solv}}(\Delta z_{\text{CTX}})$ (Figure 6b), reflecting the fact that the enthalpy of the solvent component is lost upon protein adsorption. The slopes of $\Delta H(\Delta z_{\text{CTX}})/\Delta A(\Delta z_{\text{CTX}})$ were -32.4 ± 0.3 ($R^2 = 0.993$) and -29.6 ± 0.2 ($R^2 = 0.994$) kJ/mol/nm² for the SAM and solvent components, respectively. The intercepts were chosen to be zero because there is no interaction energy between CTX and SAMs when the CTX does not contact the SAMs. These results suggest that the enthalpy is strongly and linearly correlated to the contact area for all SAM surfaces with different mixed ratios of C5 and C9. Hence, the enthalpy profiles of CTX adsorption for different components can be estimated based on the contact surface area by applying the linear relationship.

The overall entropic and enthalpic contributions to the adsorption free energy are shown by green and red bars in Figure 7a. Entropy is shown to play a greater role in the driving force relative to enthalpy, as indicated by a larger green area compared to the red area. This finding is consistent with the generally accepted concept that protein adsorption is an entropy-driven process.^{4,6,8} CTX is a highly stable protein and does not undergo unfolding during adsorption processes. Thus, the changes in the surface area of CTX during the adsorption process are also small. We have shown that the enthalpy is strongly correlated to the contact area. Therefore, the enthalpic contribution to the adsorption free energy is small for CTX adsorption. As shown in Figure 7a, the entropic contributions to adsorption affinity are similar for various SAMs (i.e., 0.8-, 1.2-, and 1.0-fold difference relative to pure C5 SAMs at mixing ratios of 0.25, 0.5, and 0.75, respectively). However, the enthalpic contributions to adsorption affinity are higher for mixed SAMs (i.e., 1.6-, 1.6-, and 3.1-fold difference relative to pure C5 SAMs at mixing ratios of 0.25, 0.5, and 0.75, respectively). These results indicate that the enhancement of the adsorption free energy on mixed SAMs results from the increase in enthalpy. The disordered topography of mixed SAMs enhances the adsorption enthalpy and thus increases the adsorption free energy. The enthalpic and entropic components are further split into the components attributed to the SAMs and the solvent: ΔH_{SAM} , ΔH_{Solv} , $-T\Delta S_{\text{SAM}}$, and $-T\Delta S_{\text{Solv}}$, as shown in Figure 7b,c.

The favorable component from SAMs for CTX adsorption mainly results from enthalpy, as shown in Figure 7b (negative ΔH_{SAM} values). Greater enthalpy is obtained for mixed rather than pure SAMs, which is consistent with our previous observations,⁵⁵ i.e., that the adsorption enthalpy was enhanced by using mixed SAM surfaces. However, the entropic component from SAMs is unfavorable (positive $-T\Delta S_{\text{SAM}}$ values) for CTX adsorption. The translational freedom of CTX and the conformations of both CTX and SAM molecules are limited when CTX is adsorbed onto SAMs. This leads to a negative contribution of SAMs to the adsorption, which was also observed in surfactant adsorption studies by Xu et al.⁵⁹ For SAMs having $\chi_{\text{C9}} = 0.25$ and 0.75, the numbers of C5 and C9 molecules are not equal, which leads to an inhomogeneous topography. Although the inhomogeneous topography increases the surface area that is in contact with CTX and leads to the favorable enthalpic change, it also limits the conformational degrees of freedom of both the CTX and SAM molecules and causes an increase in the entropic cost of CTX adsorption. Therefore, the value of ΔF_{SAM} reaches a maximum when $\chi_{\text{C9}} = 0.5$.

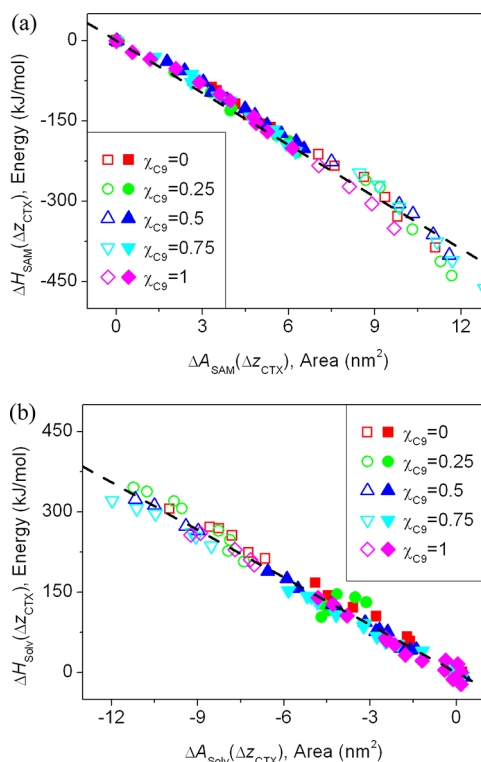


Figure 6. The change in enthalpy ($\Delta H_{\text{SAM/Solv}}$) as a function of the change in contact area ($\Delta A_{\text{SAM/Solv}}$) between the CTX molecule and the (a) SAMs and (b) the solvent. The open symbols indicate the 1st stage, and the solid symbols indicate the 2nd and 3rd stages of the CTX adsorption process.

$\Delta H_{\text{Solv}}(\Delta z_{\text{CTX}})$ are linearly correlated to $\Delta A_{\text{SAM}}(\Delta z_{\text{CTX}})$ and $\Delta A_{\text{Solv}}(\Delta z_{\text{CTX}})$. The open symbols indicate the adsorption processes in the first stage, and the solid symbols indicate the second and third stages. All three loops of CTX are attached to SAM surfaces in the first stage, only Loop I departed from the SAM surface in the second stage, and all loops are a distance from the SAM surface in the third stage. The results show that the slopes of $\Delta H(\Delta z_{\text{CTX}})/\Delta A(\Delta z_{\text{CTX}})$ are very similar at different stages of the adsorption process. The values of $\Delta H_{\text{SAM}}(\Delta z_{\text{CTX}})$ decrease with increasing $\Delta A_{\text{SAM}}(\Delta z_{\text{CTX}})$ (Figure 6a), thereby indicating that the SAM components

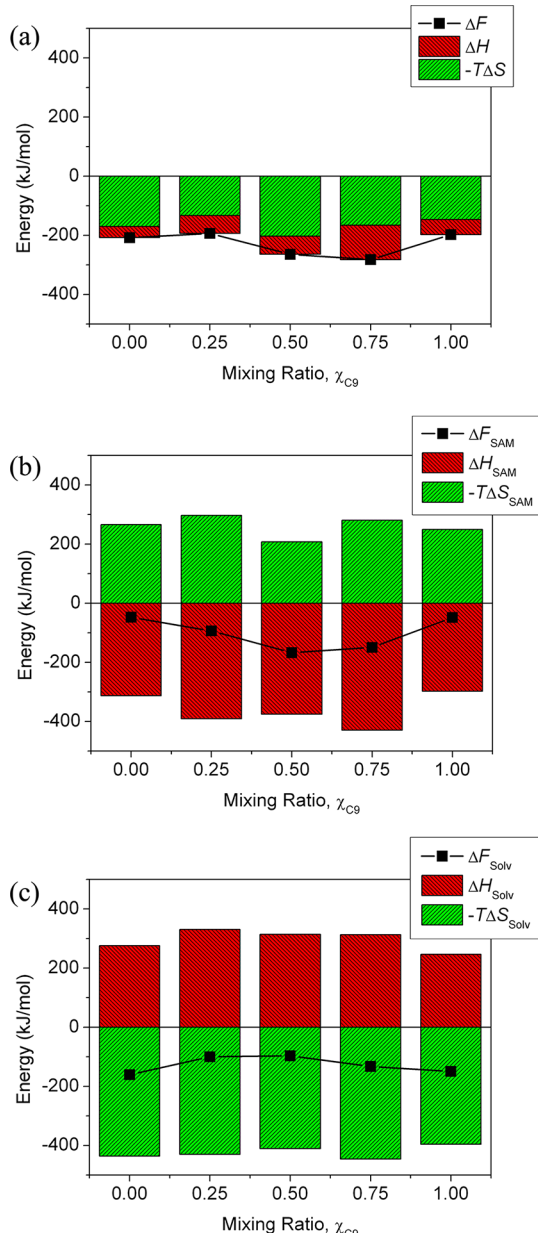


Figure 7. Changes in the free energy (black), entropy (green), and enthalpy (red) of the adsorption process as a function of the mixing ratio of C5 and C9: (a) total; (b) contribution of the SAMs; and (c) contribution of the solvent.

The favorable contribution of the solvent to CTX adsorption is attributed to entropy, as shown in Figure 7c. The unfavorable change in enthalpy (positive values in ΔH_{Solv}) for the solvent is a result of the decrease in the solvent-exposed surface area of CTX (ΔA_{Solv}) (Figure 6), i.e., the desolvation effect.⁵⁷ Because the total change in the surface area of CTX is small, the increase in ΔA_{SAM} is approximated by the decrease in ΔA_{Solv} , i.e., $\Delta A_{Solv} \sim -\Delta A_{SAM}$. Therefore, ΔH_{Solv} is almost a mirror image of ΔH_{SAM} such that ΔH_{Solv} is less favorable for mixed SAMs than that for pure SAMs. It has been suggested that the hydrophobic interaction results from the entropy increase of the ordered water molecules around the hydrophobes returning to the bulk solution when two hydrophobes come together.⁶⁰ Thus, the favorable entropic contribution from the solvent component (negative $-T\Delta S_{Solv}$ values) is due to the hydro-

phobic interaction. The contributions of $-T\Delta S_{Solv}$ are similar for each of the SAMs, and therefore, the values of ΔF_{Solv} for pure SAMs are greater due to the less unfavorable ΔH_{Solv} . Moreover, the values of $-T\Delta S_{Solv}$ are greater than that of ΔH_{SAM} , thereby indicating that the hydrophobic interaction is the dominant mechanism for CTX adsorption, which is consistent with experimental observations.^{4,6–10}

CONCLUSIONS

In this paper, MD simulations and PMF calculations were performed to identify and characterize the mechanisms of adsorption for a protein on designed surfaces. The thermodynamic properties, such as the free energy, enthalpy, and entropy, as well as conformation changes were determined for the model systems that were comprised of a single CTX molecule and a set of mixed SAM surfaces. The mixed SAMs were created by mixing *n*-alkanethiols with two different chain lengths (C5 and C9).

This study illustrated that CTX undergoes similar conformational changes, although the detachment distances and adsorption affinities are different for CTX adsorption onto SAMs with different mixing ratios (χ_{C9}). It was shown that the adsorption affinities for mixed SAMs with mixing ratios $\chi_{C9} = 0.5$ and 0.75 were approximately 35% higher than those of the other SAMs. These results are in agreement with the atomic force microscopy measurements demonstrating that the adhesion forces of CTX on mixed SAMs were greater than those on pure SAMs.

The component analysis was implemented to achieve two goals: to distinguish between the effects of SAMs and the solvent on CTX adsorption and to identify the major thermodynamic functions acting on the adsorption process. The component analysis of the effects of SAMs and the solvent revealed that the percentages of solvent component of overall adsorption free energy were 77% and 76% for pure SAMs with $\chi_{C9} = 0$ and 1, respectively, but were 52%, 37%, and 47% for mixed SAMs with $\chi_{C9} = 0.25$, 0.5, and 0.75, respectively. Thus, the mixing ratios of C5 and C9 altered the relative contributions of the SAMs and the solvent to the overall driving force for CTX adsorption onto SAM surfaces. The component analysis of the thermodynamic functions showed that CTX adsorption was an entropy-driven process. The disordered topography of the mixed SAMs increased the enthalpy of CTX adsorption, thereby leading to enhanced binding affinities of CTX onto mixed SAMs. Further component analyses demonstrated that SAMs contributed enthalpy to drive CTX adsorption, the solvent contributed entropy, and the hydrophobic interaction was the driving force for CTX adsorption. In addition, the enthalpy calculation revealed that the enthalpy was strongly and linearly correlated to the contact area. In summary, the present analysis revealed that surfaces composed of a mixture of SAMs with different chain lengths enhance the adsorption affinity mainly due to increases in enthalpy. For the hydrophobic SAMs studied in the present study, the hydrophobic interaction is the major mechanism for protein adsorption. However, for the protein adsorption onto the hydrophilic and charged SAMs, the electrostatic interaction, leading to hydrogen bonds and salt bridges with proteins, will play an important role. Further studies of the free energy contribution of the electrostatic interaction are needed to investigate the mechanisms of protein adsorption onto the hydrophilic and charged SAMs.

AUTHOR INFORMATION

Corresponding Author

*E-mail: cchieng@ess.nthu.edu.tw.

Notes

The authors declare no competing financial interest.

ACKNOWLEDGMENTS

The authors thank the National Center for High-Performance Computing, Taiwan for computing resources and the National Science Council, Taiwan for financial support under Grant No. NSC99-2221-E007-028-MY2.

REFERENCES

- (1) Kasemo, B. *Surf. Sci.* **2002**, *500*, 656–677.
- (2) Thevenot, P.; Hu, W.; Tang, L. *Curr. Top. Med. Chem.* **2008**, *8*, 270–80.
- (3) Gray, J. J. *Curr. Opin. Struct. Biol.* **2004**, *14*, 110–5.
- (4) Wilson, C. J.; Clegg, R. E.; Leavesley, D. I.; Pearcy, M. J. *Tissue Eng.* **2005**, *11*, 1–18.
- (5) Love, J. C.; Estroff, L. A.; Kriebel, J. K.; Nuzzo, R. G.; Whitesides, G. M. *Chem. Rev.* **2005**, *105*, 1103–69.
- (6) Andrade, J. D.; Hlady, V. *Adv. Polym. Sci.* **1986**, *79*, 1–63.
- (7) Tilton, R.; Robertson, C. *Langmuir* **1991**, *7*, 2710–2718.
- (8) Haynes, C. A.; Norde, W. *Colloids Surf., B* **1994**, *2*, 517–566.
- (9) Ostuni, E.; Grzybowski, B. A.; Mrksich, M.; Roberts, C. S.; Whitesides, G. M. *Langmuir* **2003**, *19*, 1861–1872.
- (10) Prime, K. L.; Whitesides, G. M. *Science* **1991**, *252*, 1164–1167.
- (11) Schmidt, D. R.; Waldeck, H.; Kao, W. J. Protein Adsorption to Biomaterials. In *Biological Interactions on Materials Surfaces*; Puleo, D. A., Bizios, R., Eds.; Springer: New York, 2009; pp 1–18.
- (12) Latour, R. A. *Biointerphases* **2008**, *3*, FC2.
- (13) Raffaini, G.; Ganazzoli, F. *Macromol. Biosci.* **2007**, *7*, 552–66.
- (14) Zhang, L.; Sun, Y. *Biochem. Eng. J.* **2010**, *48*, 408–415.
- (15) Zhou, J.; Zheng, J.; Jiang, S. *J. Phys. Chem. B* **2004**, *108*, 17418–17424.
- (16) Zheng, J.; Li, L.; Chen, S.; Jiang, S. *Langmuir* **2004**, *20*, 8931–8938.
- (17) Agashe, M.; Raut, V.; Stuart, S. J.; Latour, R. A. *Langmuir* **2005**, *21*, 1103–1117.
- (18) Zheng, J.; Li, L.; Tsao, H.-K.; Sheng, Y.-J.; Chen, S.; Jiang, S. *Biophys. J.* **2005**, *89*, 158–166.
- (19) He, Y.; Chang, Y.; Hower, J. C.; Zheng, J.; Chen, S.; Jiang, S. *Phys. Chem. Chem. Phys.* **2008**, *10*, 5539–5544.
- (20) Wang, Q.; Zhao, C.; Zhao, J.; Wang, J.; Yang, J.-C.; Yu, X.; Zheng, J. *Langmuir* **2010**, *26*, 3308–3316.
- (21) Wang, Q.; Zhao, J.; Yu, X.; Zhao, C.; Li, L.; Zheng, J. *Langmuir* **2010**, *26*, 12722–12732.
- (22) Wang, Q.; Shah, N.; Zhao, J.; Wang, C.; Zhao, C.; Liu, L.; Li, L.; Zhou, F.; Zheng, J. *Phys. Chem. Chem. Phys.* **2011**, *13*, 15200–15210.
- (23) Zhao, J.; Wang, Q.; Liang, G.; Zheng, J. *Langmuir* **2011**, *27*, 14876–14887.
- (24) Kirkwood, J. G. *J. Chem. Phys.* **1935**, *3*, 300.
- (25) Chipot, C.; Mark, A.; Pande, V.; Simonson, T. Applications of Free Energy Calculations to Chemistry and Biology. In *Free Energy Calculations Theory and Applications in Chemistry and Biology*; Chipot, C., Pohorille, A., Eds.; Springer: Berlin, Germany, 2007; pp 463–492.
- (26) Kollman, P. *Chem. Rev.* **1993**, *93*, 2395–2417.
- (27) Fletcher, J. E.; Jiang, M.-S. *Toxicon* **1993**, *31*, 669–695.
- (28) Dufton, M. J.; Hider, R. C. *Pharmacol. Ther.* **1988**, *36*, 1–40.
- (29) Huang, W.-N.; Sue, S.-C.; Wang, D.-S.; Wu, P.-L.; Wu, W.-G. *Biochemistry* **2003**, *42*, 7457–66.
- (30) Forouhar, F.; Huang, W.-N.; Liu, J.-H.; Chien, K.-Y.; Wu, W.-G.; Hsiao, C.-D. *J. Biol. Chem.* **2003**, *278*, 21980–8.
- (31) Dubovskii, P. V.; Dementieva, D. V.; Bocharov, E. V.; Utkin, Y. N.; Arseniev, A. S. *J. Mol. Biol.* **2001**, *305*, 137–49.
- (32) Dubovskii, P. V.; Lesovoy, D. M.; Dubinnyi, M. a.; Konshina, A. G.; Utkin, Y. N.; Efremov, R. G.; Arseniev, A. S. *Biochem. J.* **2005**, *387*, 807–15.
- (33) Efremov, R. G.; Volynsky, P. E.; Nolde, D. E.; Dubovskii, P. V.; Arseniev, A. S. *Biophys. J.* **2002**, *83*, 144–53.
- (34) Su, Z.-Y.; Wang, Y.-T. *J. Phys. Chem. B* **2011**, *115*, 796–802.
- (35) Levtsova, O. V.; Antonov, M. Y.; Mordvintsev, D. Y.; Utkin, Y. N.; Shaitan, K. V.; Kirpichnikov, M. P. *Comput. Biol. Chem.* **2009**, *33*, 29–32.
- (36) Sue, S.-C.; Jarrell, H. C.; Brisson, J. R.; Wu, W.-G. *Biochemistry* **2001**, *40*, 12782–94.
- (37) Szőri, M.; Jedlovszky, P.; Roeselová, M. *Phys. Chem. Chem. Phys.* **2010**, *12*, 4604–4616.
- (38) Rudich, Y.; Benjamin, I.; Naaman, R.; Thomas, E.; Trakhtenberg, S.; Ussyshkin, R. *J. Phys. Chem. A* **2000**, *104*, 5238–5245.
- (39) Bumm, L. A.; Arnold, J. J.; Charles, L. F.; Dunbar, T. D.; Allara, D. L.; Weiss, P. S. *J. Am. Chem. Soc.* **1999**, *121*, 8017–8021.
- (40) Smith, R. K.; Lewis, P. A.; Weiss, P. S. *Prog. Surf. Sci.* **2004**, *75*, 1–68.
- (41) Chen, S.; Li, L.; Boozer, C. L.; Jiang, S. *Langmuir* **2000**, *16*, 9287–9293.
- (42) Efremov, R. G.; Nolde, D. E.; Konshina, A. G.; Syrtcev, N. P.; Arseniev, A. S. *Curr. Med. Chem.* **2004**, *11*, 2421–42.
- (43) Lomize, M. A.; Lomize, A. L.; Pogozheva, I. D.; Mosberg, H. I. *Bioinformatics* **2006**, *22*, 623–5.
- (44) Van Der Spoel, D.; Lindahl, E.; Hess, B.; Groenhof, G.; Mark, A. E.; Berendsen, H. J. C. *J. Comput. Chem.* **2005**, *26*, 1701–18.
- (45) Hautman, J.; Klein, M. L. *J. Chem. Phys.* **1989**, *91*, 4994.
- (46) Tupper, K. J.; Brenner, D. W. *Langmuir* **1994**, *10*, 2335–2338.
- (47) Berendsen, H. J. C.; Grigera, J. R.; Straatsma, T. P. *J. Phys. Chem.* **1987**, *91*, 6269–6271.
- (48) Nose, S. *J. Chem. Phys.* **1984**, *81*, 511.
- (49) Hoover, W. G. *Phys. Rev. A* **1985**, *31*, 1695–1697.
- (50) Hess, B.; Bekker, H.; Berendsen, H. J. C.; Fraaije, J. G. E. M. *J. Comput. Chem.* **1997**, *18*, 1463–1472.
- (51) Beck, D. A. C.; Armen, R. S.; Daggett, V. *Biochemistry* **2005**, *44*, 609–16.
- (52) Steinbach, P. J.; Brooks, B. R. *J. Comput. Chem.* **1994**, *15*, 667–683.
- (53) Hung, S.-W.; Hsiao, P.-Y.; Chieng, C.-C. *J. Chem. Phys.* **2011**, *134*, 194705.
- (54) Torrie, G. M.; Valleau, J. P. *J. Comput. Phys.* **1977**, *23*, 187–199.
- (55) Hung, S.-W.; Hsiao, P.-Y.; Chieng, C.-C. *IEEE Trans. Nanobiosci.* **2010**, *9*, 297–306.
- (56) Chang, J.-M.; Tseng, F.-G.; Chieng, C.-C. *IEEE Trans. Nanobiosci.* **2010**, *9*, 289–96.
- (57) Levy, R. M.; Zhang, L. Y.; Gallicchio, E.; Felts, A. K. *J. Am. Chem. Soc.* **2003**, *125*, 9523–30.
- (58) Eisenhaber, F.; Lijnzaad, P.; Argos, P.; Sander, C.; Scharf, M. *J. Comput. Chem.* **1995**, *16*, 273–284.
- (59) Xu, Z.; Yang, X.; Yang, Z. *J. Phys. Chem. B* **2008**, *112*, 13802–11.
- (60) Ball, P. *Chem. Rev.* **2008**, *108*, 74–108.
- (61) DeLano, W. L. The PyMOL Molecular Graphics System, Version 0.99, 2008.